Progress in Propulsion Physics **2** (2011) 3-20

ISSUES RELATED TO HETEROGENEOUS SOLID-PROPELLANT COMBUSTION

T. L. Jackson

University of Illinois at Urbana-Champaign
Urbana, IL 61801, USA

Over the past decade, a considerable amount of efforts has been dedicated to computational simulations of heterogeneous solid-propellant combustion. A variety of tools have emerged from those studies. The most important are the modeling of propellant morphology, homogenization, and an unsteady three-dimensional (3D) combustion code with complete coupling of the gas-phase combustion processes and the solid-phase heat conduction across the unsteadily regressing nonplanar propellant surface. The combustion code is both parallel and scalable. These tools have been applied to the study of both nonaluminized and aluminized (conventional size Al and nano-Al) heterogeneous propellants. A number of important problems will be reviewed using these tools.

1 INTRODUCTION — THE BASIC MODEL

Over the past decade, much effort has been dedicated to computational simulations of heterogeneous solid-propellant combustion. Researchers have been concerned with the combustion of heterogeneous propellants and their interaction with the chamber flow.

This work has a number of ingredients, the most important of which are: a random-packing model of the propellant that simulates particles of oxidizer embedded in fuel–binder; homogenization into an oxidizer/fuel blend of particles too small to be numerically resolved; unsteady 3D heat conduction within the solid that takes into account material properties of the different ingredients; a gas-phase description using the zero Mach-number Navier–Stokes equations and global kinetics; a representation of the propellant surface that is either explicit or implicit (via a level-set strategy); a full coupling between the solid and the gas across the surface; and the ability to account for the presence of aluminum particles. The complete code can predict the effects of morphology on burning rates; provide insights into the nature of the combustion field; calculate the amplitude and phase-shift of an acoustic wave impinging on the burning propellant,

Article available at http://www.eucass-proceedings.eu or http://dx.doi.org/10.1051/eucass/201102003

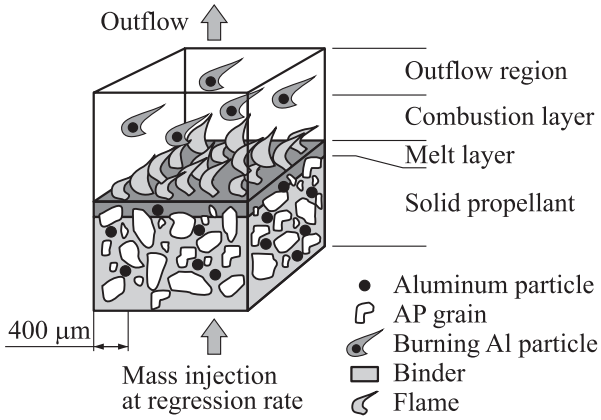

Figure 1 A cartoon of the combustion field

a matter of great importance in rocket chamber stability; predict the velocity and temperature fluctuations on the millimeter scale above the surface, boundary conditions for large-eddy simulations (LES) of the chamber flow; provide a foundation for a rational one-dimensional (1D) description of the combustion field, needed for whole-rocket simulations on large length scales; provide a framework for modeling aluminum agglomeration; and provide a framework for erosive burning investigations of both homogeneous and heterogeneous propellants.

These topics will be presented here and in the following sections.

Figure 1 is a cartoon of the combustion system and gives some sense of its complexity. In examining this figure, it is clear that the first thing one needs to do is create a model of the propellant morphology, the distribution of ammonium perchlorate (AP) particles and aluminum (Al) particles in the binder. This can be done using a dynamic random packing algorithm [1], assuming that all particles can be represented by spheres, a reasonable approximation when the propellant is statistically isotropic [2]. A pack generated in this way is shown in Fig. 2 [4–6].

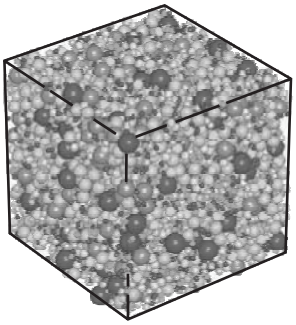

Figure 2 A 10.001 particle pack that models the Miller M21 pack [3]. The pack consists of by weight 87.4% AP and 12.6% binder; size and size distribution from Miller data

The distribution of AP particle sizes used in practice is large, from hundreds of microns

down to a micron. The smaller particles cannot be resolved numerically, and yet, they may constitute a significant volume fraction and so should not be neglected. The proper way to account for them is to homogenize them into the binder to create a homogeneous blend of binder and AP. The properties of this blend are calculated using homogenization theory [7].

With a model for the morphology in place, the next step is to construct field equations for the solid and the gas. In the solid, one has simple heat conduction, albeit with different conductivities and densities for the different components. The gas flow is a small Mach-number flow, and the important question there is the modeling of the chemical kinetics. Global schemes, unavoidable given the computational challenges, either 2- or 3-step were used. The 3-step model is appropriately called the Beckstead–Derr–Price (BDP) model: AP decomposition; reaction between the AP gases and the binder gases (the so-called primary diffusion flame); and reaction between the products of AP decomposition and the binder gases (the so-called secondary diffusion flame). The difficulty with any global model lies in specifying the various parameters: they must be determined by empirical fits, and yet, it would be foolish to fit, say, burning rate data for heterogeneous propellants, as that is precisely one of the things one would like to predict, and curve-fitting hardly needs a challenging computation carried out on thousands of processors. For this reason, when one appeals to burning-rate data, one only uses 1D data, that for pure AP or for a homogeneous blend of AP and binder [8, 9].

The final step is a description of the propellant surface; and here there are two strategies. For Al-free propellants, it is typically the case that the surface can be specified by a single-valued function

$$y = f(x, z, t)$$

and then f satisfies the kinematic equation

$$f_t + r_b\sqrt{1 + (f_x)^2 + (f_z)^2} = 0$$

where r_b is the regression speed of the surface. For aluminized propellants, the surface cannot be so described at parts of the surface defined by Al, and then, a level-set strategy is needed [10–12]. But in either case, it is assumed that the complex physics and chemistry that occurs in a thin surface layer of the propellant can be modeled by a simple pyrolysis law:

$$r_b = A_s \exp\left(-\frac{E_s}{RT_s}\right)$$

where T_s is the surface temperature.

When all of these ingredients are put together, it is possible to predict the burning rate of a heterogeneous propellant. The author is greatly indebted to

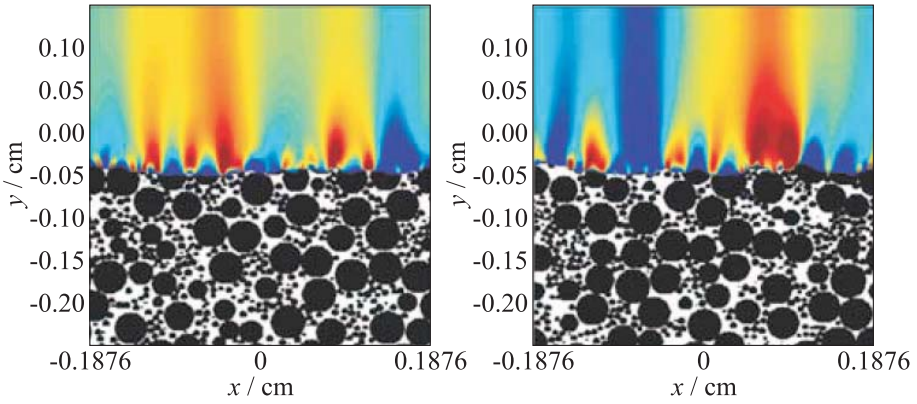

Figure 3 Normal velocity (cm/s) on two different vertical slices through the pack. The color bar ranges from 500 (red) to 250 (blue) cm/s: (*a*) $z = 0.0454$ cm; and (*b*) $z = 0.1402$ cm. (Refer Jackson, p. 6.)

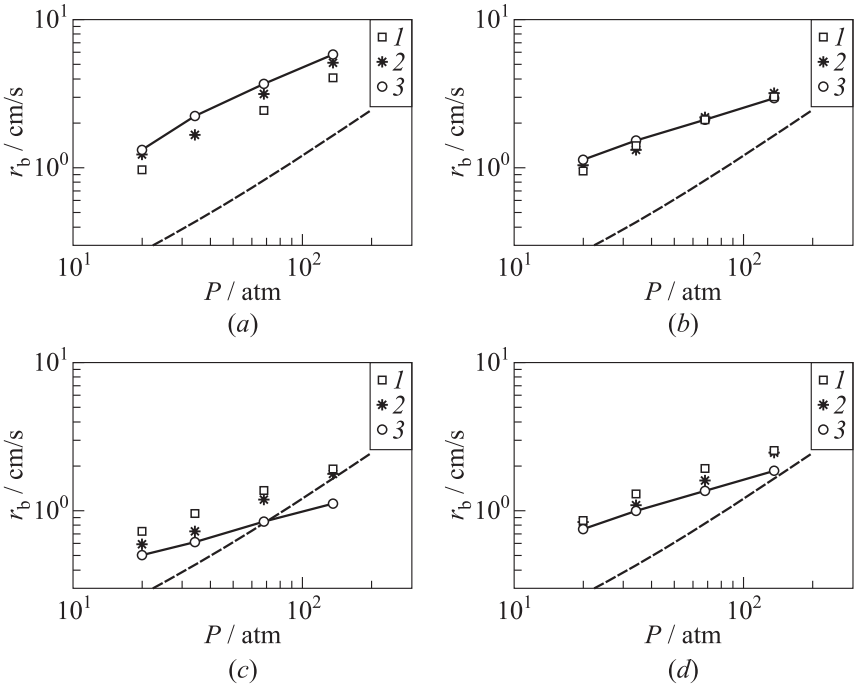

Figure 4 Burning-rate predictions (*1* — 2-step kinetics; and *2* — 3-step kinetics using the BDP model) compared to Miller's experimental data (*3*): (*a*) M03; (*b*) M17; (*c*) M21; and (*d*) M24

R. Miller who, some years ago, created a number of propellant packs, recorded their statistics (size distributions) and burnt them over a range of pressures, measuring their burning rates [3]. For certain nonaluminized examples, model packs with the same distributions as the real ones have been constructed and numerically burnt. Figure 3 shows the normal velocity component for two different vertical cuts through the combustion field and includes a part of the propellant pack. The color-bar corresponds to speeds in the range of cm/s (blue) to 500 cm/s (red), and shows a variation of about 50% in the normal velocity along the propellant surface; similarly, variations of about 20% are observed in the temperature [13]. Comparisons between the predictions and the experiments are shown in Fig. 4 [8]. As a final comment here, note that the fully coupled, 3D solid–gas numerical code, using 2.5 million grid points, takes approximately 16 wall clock hours on 96 processors per 1 mm of burning.

This is not the place to discuss these comparisons in detail, but the agreement using the 3-step model is quite acceptable except for the pack M21, and there is a reason to question the experimental data [8]. Note that at fixed pressure, changes in the burning rate with morphology are significant, and these changes are captured by the simulations.

2 ALUMINIZED PROPELLANTS

It is commonplace to use Al in high-performance propellants, for this improves the specific impulse. Aluminum burns in the water vapor and carbon dioxide which are the products of the oxide/binder reactions. It is much harder to simulate aluminized propellants than those sans Al because, as was already noted, a level-set strategy is required. Only recently such a strategy was implemented, and Fig. 5 shows a result obtained during preliminary explorations [12]. One interesting feature of solutions such as these is that they show that the larger Al particles tend to linger near the surface following detachment, and drift horizontally due to aerodynamic forces. This behavior has been seen experimentally. For the modeling of fine or ultra-fine Al, the interested reader should consult [14].

Important physics missing at the present time is relevant to the behavior of the Al after it reaches the surface and before it detaches. Each particle lingers for a few microseconds in a melt layer at the binder surface, and, during that time period, agglomeration occurs. Particle diameters in the pack are typically in the neighborhood of 20 μm, but agglomerates of diameter 100–200 μm can form, and these are a problem for the rocket designer. Amongst other things, they can impinge (after oxidation) on the nozzle walls, scouring them; and in the case of reentrant nozzles, they can accumulate behind the nozzle lip, significant dead weight that is deleterious to performance. An understanding of agglomeration is a high priority for the industry.

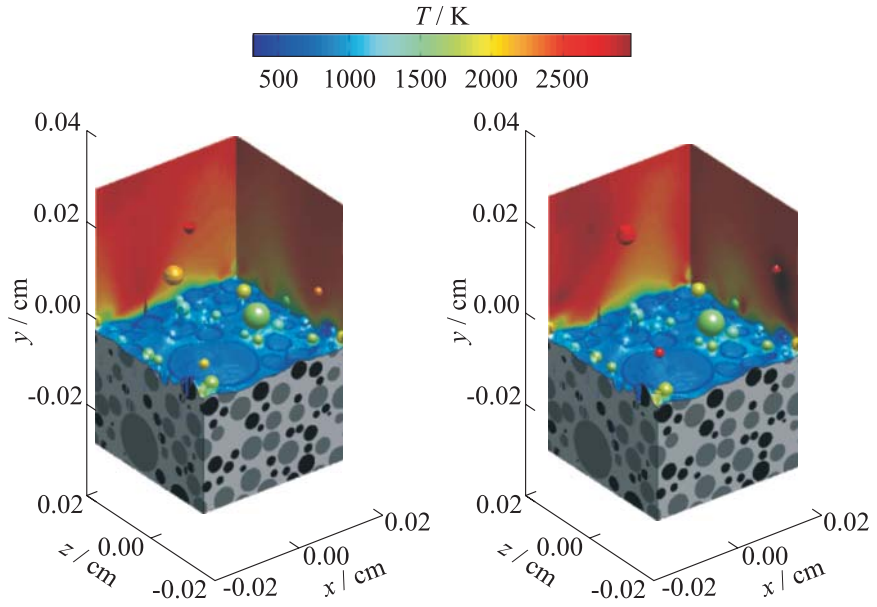

Figure 5 Surface topography and temperature level-surfaces for a sample propellant; pressure = 20 atm. Times are $t = 4.2$ ms (a) and $t = 4.3$ ms (b). (Refer Jackson, p. 8.)

Two issues relevant to agglomeration are discussed in [15]: melting and drift in the melt layer.

Agglomeration can probably only occur if the particles have melted. Aluminum melts at a temperature of 933 K, which is comparable to the surface temperature of the propellant, and so one would reasonably expect that large particles will not melt, whereas small particles will. This is something that, for the first time, can be directly tested via numerical simulations, and what is found, for sizes used in practice, is that melting might not have occurred when the particle first emerges, but certainly has occurred when emergence is complete.

As for drift in the melt layer, an elementary model has been constructed which assumes that drift occurs because of surface tension gradients, so that a particle will move towards a temperature minimum. Using the simulations, one can calculate the location of all such minima at the binder surface and construct their loci. If the particles can keep up with the motion of the minima, the history of these loci is a measure of the particle drift. By averaging over all of the loci, one can say something about the drift, and Fig. 6 shows the typical results. The

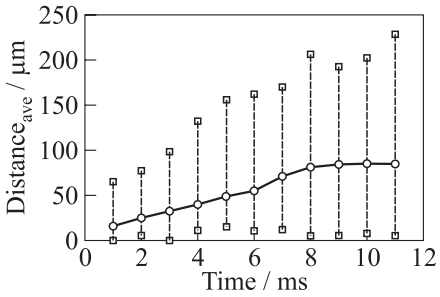

Figure 6 Accumulated drift of temperature minima at the HTPB surface: middle — average; top — greatest; bottom — least

distance moved from the original location is approximately a ramp function. Thus, while drift is occurring, there is a well-defined drift velocity, but the drift is capped. The latter is a "pocket effect" — drift is constrained by the presence of the AP particles, here to a maximum of approximately 80 μm.

3 FLUID DYNAMIC ISSUES

The propellant combustion plays an important role in defining the chamber flow of course, and there are two issues that were examined: the reflection of an acoustic wave from the burning surface; and flow perturbations at distances of a millimeter or so from the surface. The first question is important for stability considerations, as the wave can be amplified, and if the sum of such amplifications as the acoustic wave bounces around the chamber is greater than accumulated losses, nonlinear vibrations will occur, often violent in nature. The second question is important for the calculation of the turbulent flow field in the chamber, for it defines boundary conditions for LES calculations.

3.1 Pressure Fluctuations

There are actually two kinds of instability that are driven by chamber disturbances, specifically pressure disturbances. One is the so-called L^*-instability, which can occur for small rockets, and is associated with mass-flux imbalances in the chamber (L^* is the ratio of the chamber volume to the nozzle throat area). Here, what is relevant is the fluctuation in the mass flux from the propellant surface due to a local fluctuating pressure. The second is the amplification of a pressure disturbance, and what is relevant is the fluctuation in the velocity from the surface due to a local fluctuating pressure. The mass flux response function R is defined by

$$\frac{m'}{m} = \frac{Rp'}{p}$$

and is "easily" measured in an experiment. Instability can occur if the real part of R is greater than 1 (there are also conditions on L^*). The velocity response function is related to fluctuations in the energy flux, viz.

$$\frac{(mT)'}{mT} = \frac{Sp'}{p}; \quad \frac{v'}{v} = \frac{(S-1)p'}{p}$$

and is difficult to measure. Instability can occur if the real part of S is greater than 1. It is often assumed that R and S differ little, if at all, and this is an assumption that can be evaluated numerically.

The response of a homogeneous propellant, a 1D problem, is easily examined via analytic or quasi-analytic means, and leads to single-peaked response functions. A question not clearly understood is whether multiple peaks are possible for heterogeneous propellants, and this also can be evaluated numerically.

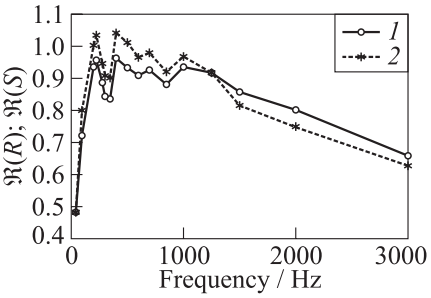

Figure 7 Pressure response functions for a heterogeneous propellant (monomodel, pressure = 60 atm): *1* — $\mathcal{R}(R)$; and *2* — $\mathcal{R}(S)$

Both questions identified here have been examined in [16], albeit for a two-dimensional (2D) propellant. Figure 7 shows the results for one set of calculations reported in [16]. This shows the real part of R and of S for a monomodal pack of 100-micron AP particles in binder (no Al) burning at a pressure of 60 atm. When only a single peak in the real part of S occurs (greater than 1), it is argued that the frequency defined by the peak characterizes the waves that will grow most rapidly, and so will characterize the nonlinear consequences of the instability. When there are multiple peaks (greater than 1), multiple modes will be amplified. For other packs examined in [16], the real part of R is also greater than 1 for some frequencies, with the possibility of L^*-instability.

3.2 Flow Fluctuations Above the Surface

There is a reason to believe that, at least in some part of the rocket chamber, there is a two-way interaction between the fluctuations in the chamber and the fluctuations in the thin combustion layer just above the propellant. The effect of the chamber fluctuations on the burning has to be studied and understood

yet, but the effect of burning fluctuations on the chamber flow has been already examined [13].

The natural time scale for the solid physics is much longer than that for the gas physics, and therefore, the only concern here is a quasi-steady gas phase for which temporal changes only occur because of temporal changes at the propellant surface. These evolve as distance from the surface increases, and a relevant question is: at what distance from the surface the combustion field has no effect, so that the fluctuations can be used as boundary conditions for the chamber flow? This can be determined by examining the divergence of the velocity field, and for the calculations of [13], a distance of 0.5 mm is arrived at. None of earlier calculations (see, e. g., [8]) require integration to such distances, as the heat flux to the surface (which controls the burning rate) is controlled by the layer within tens of microns of the surface.

At this half millimeter level, it is possible to determine the complete statistics of the fluctuations. Not surprisingly, the spatial correlations in a plane parallel

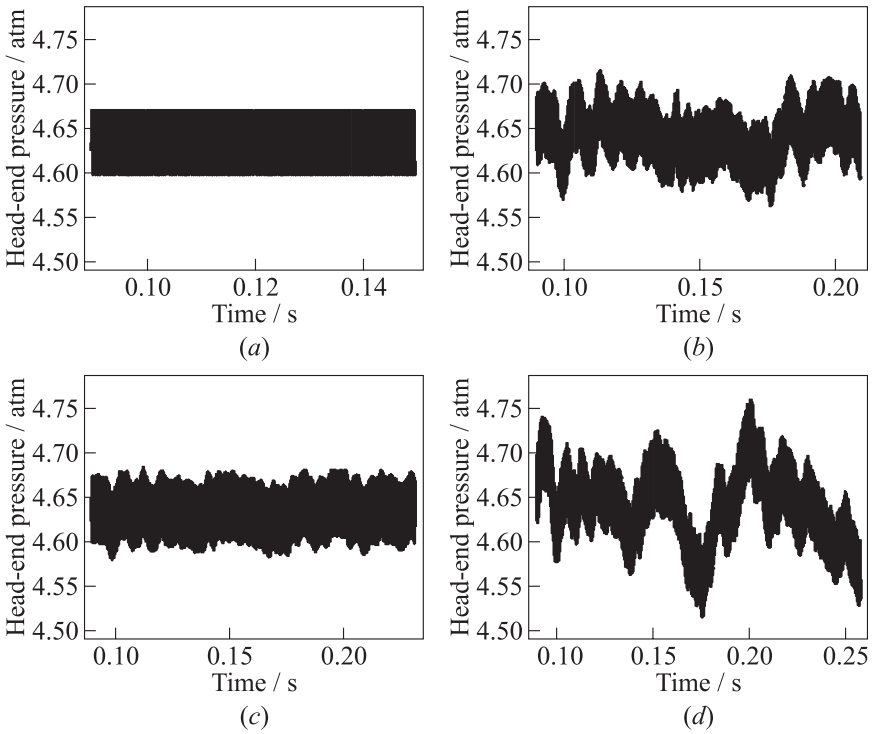

Figure 8 Head-end pressure fluctuations for no surface fluctuations (a), and for three propellants for which there are surface fluctuations: (b) Th20_50_200; (c) P82; and (d) P82_390

to the surface are negligible on any scale relevant to the chamber flow (smallest mesh size). However, the temporal correlations are not negligible, and these can have an effect.

One issue that is of interest to the rocket designer are the fluctuations that occur in the head-end pressure. For large rockets, these can be substantial, and there are fatigue consequences. The fluctuations that occur in a small rocket, the so-called Onera C1 rocket, a model configuration frequently used in numerical simulations, with a length of approximately 1 m has been examined. Figure 8 shows head-end pressure fluctuations with time (seconds) for several propellants (e. g., one labeled P82, Fig. 8*c*), compared to the fluctuations when the efflux from the propellant is assumed to be steady (Fig. 8*a*). The fluctuations in this last case, which define a thick band on the seconds scale, are acoustic oscillations (the fundamental frequency) on a scale of approximately 50 ms. More recent numerical simulations investigating the effect of propellant morphology on the acoustics in a planar rocket motor can be found in [17]. The computations presented here are 2D, and may overpredict the amplitudes. The author is in the process of carrying out 3D simulations and will report on them in due time.

3.3 One-Dimensional Models

Almost all of the modeling of heterogeneous propellant combustion carried out prior to the work at CSAR is 1D — the equations for a homogeneous propellant are used, with suitable average properties. Such a strategy is seriously flawed on two accounts: when the 3D equations are averaged over a plane parallel to the propellant surface for the purposes of generating, a 1D description, terms analogous to the Reynolds stress terms that arise in ensemble averaging of the Navier–Stokes equations are generated; and no 1D gas-phase description can decently capture the role played by the mix of deflagrations and diffusion flames that occur in three dimensions.

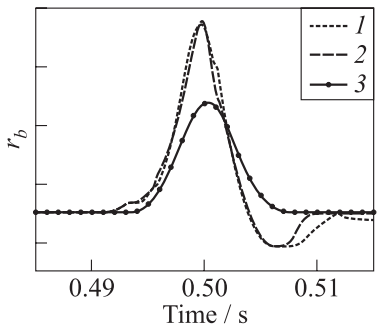

Figure 9 Response to a pressure pulse, burning rate r_b vs. time

There is need for a 1D description, however. In whole rocket simulations from ignition to burnout, there are substantial changes in the chamber pressure, and these strongly affect the burning rate. But because of the enormous difference between the length scale of the chamber flow and the length scale of the combustion field, the two codes cannot be directly coupled. The chamber flow "sees" a homogeneous propellant. The way in which the code identified in [8] can be

used to generate an equivalent 1D model which can be coupled with the flow code is described in [18]. Figure 9 shows a test case, the response of the burning to a pressure pulse. The solid curve *1* is the response calculated using the full 3D code; the broken line *2* is the response calculated using the equivalent 1D code. The solid line *3* corresponds to the usual model of Ap^n; note that the standard quasi-steady model does not predict the dynamics, especially the undershoot. Key components of the 1D code include a large lookup table generated using the 3D code, and modeling of the Reynolds stress terms that arise upon averaging.

3.4 Erosive Burning

Propellants of solid rocket motors (SRM) are the subject to intense time-dependent shear flows, and the response of the combustion field to these flows is of fundamental interest. In addition, the flow perturbations that are generated can modify the acoustic field within the chamber and, because of the two-way coupling, lead to violent instabilities. There are a number of possible mechanisms that can give rise to time-dependent shear flows, namely, acoustics, surface irregularities, and turbulence. For example, it has been shown that interaction between axial acoustic waves and the vortical mean flow can generate large time-dependent shear flows in the vicinity of the propellant surface [19–21]. An estimate of the shear rate in the presence of acoustic waves is $2.7 \cdot 10^5$ s^{-1} [20]. It is believed that these intense time-dependent shear flows near the propellant surface can lead to the phenomena called "erosive burning," a modification of the local burn rate from its strand burn rate. There are two issues: (*i*) estimating the amplitude of the shear rate near the propellant surface, and (*ii*) determining the effect of shear on the combustion of solid propellants. In the next subsection, a method for determining the amplitude of the shear based on a multiscale approach is presented. Then the shear profile near the propellant surface is examined. Based on these findings, appropriate models for the shear are then developed for both homogeneous and heterogeneous propellants.

Multiscale rocket chamber analysis

Estimating the flow dynamics near the propellant surface requires full-scale SRM simulations to be carried out. However, these simulations are expensive both in terms of CPU costs and in wall clock time. An alternative is to use a multiscale analysis which is based on the assumption that both the mean flow and the turbulent fluctuations evolve slowly in the axial direction. It has been formulated and used by Spalart for turbulent boundary layers [22] and by Venugopal *et al.* [23] (and references therein) for planar SRM computations. Within the SRM context, it determines the flow dynamics at any plane with streamwise location

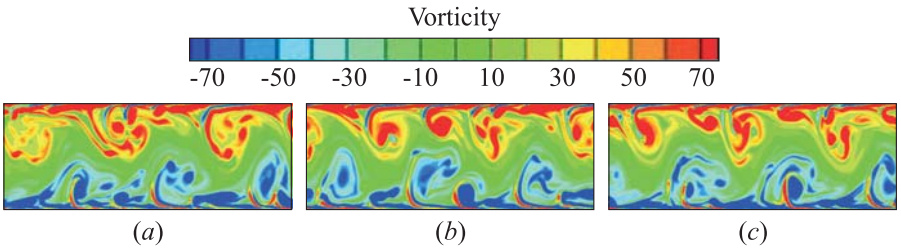

Figure 10 Results from multiscale analysis for planar geometry and for $\mathrm{Re}_{\mathrm{inj}} = 1000$ and $\varepsilon = 0.04$. Vorticity fields in domain $[0 : 4\pi] \times [-1 : 1]$ at three different instants of time: (a) T; (b) $T + 2$; and (c) $T + 4$. (Refer Jackson, p. 14.)

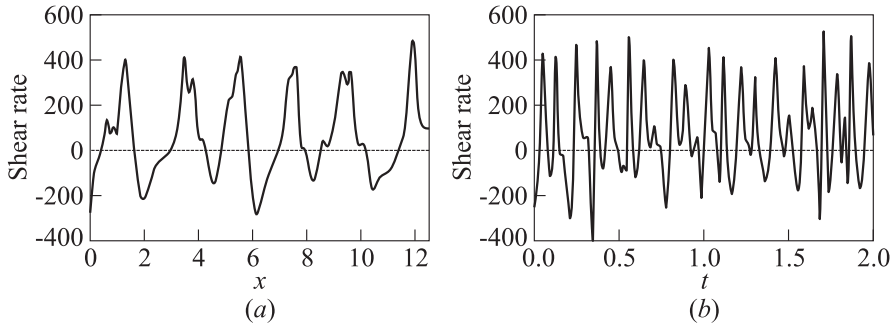

Figure 11 Shear rate near propellant surface as a function of space at one instant of time $T + 4$ (a) and as a function of time at one location $x = 2\pi$ (b)

$x/h = 1/\varepsilon$ where ε is a small parameter; x is the distance from the head-end; and h is the half-width (radius) of the chamber for a planar (cylindrical) geometry. Asymptotic analysis valid in the limit of vanishing ε removes the overall axial gradients and generates a problem with periodic boundary conditions at the upstream and downstream ends in which the gradient effects appear as source terms in the evolution equations [23]. Despite ε is a geometric parameter, it is also the ratio of mass injection rate to the mean flow rate [23] at the location x/h.

The multiscale analysis leads to a set of nondimensional conservation equations with source terms that arise as a result of the multiscale expansion in ε. These equations are then solved numerically, and selective results are shown in Figs. 10 and 11 for a 2D plane geometry. Shown in Fig. 10 are spanwise vorticity contours at three different instants of time. The nondimensional shear rate is plotted in Fig. 11a as a function of space at one instant of time, and plotted in Fig. 11b as a function of time at one location. In dimensional values and for a particular motor geometry, one finds that the dimensional wavelength asso-

ciated with Fig. 11*a* is on the order of millimeters, too large to have an effect on the combustion dynamics of heterogeneous propellants (length scales on the order of microns), but can have an effect on homogeneous propellants. The shear amplitudes in dimensional units can be as large as 10^5 (1/s), of the same order as that observed in recent numerical simulations [20]. The corresponding frequencies can be estimated from Fig. 11*b*, and typically lie in the range of a few hertz up to the kilohertz range. These observations allow developing appropriate models of the velocity field near the propellant surface, and then investigating its influence on the combustion process of both homogeneous and heterogeneous propellants. Therefore, it is now possible to develop a unified theory for erosive burning in both heterogeneous and homogeneous propellants. Similar results are obtained for axisymmetric and 3D cylindrical geometries.

Homogeneous propellants

As mentioned, the velocity field from the multiscale formulation near the propellant surface was examined and significant shear rates of the same order as those found in full scale numerical simulations of solid rocket motors were shown to exist and to exhibit a spatial dependence. The typical wavelength from the multiscale analysis is too large to have any influence on the scales of a heterogeneous propellant (millimeters vs. microns), but can affect the flow field for a homogeneous propellant. Therefore, for a homogeneous propellant, the velocity field near the propellant surface is modeled as solenoidal, namely,

$$u = A \sin\left(\frac{2\pi}{\lambda} x\right) y\,; \quad v = 1 - \frac{A\pi}{\lambda} \cos\left(\frac{2\pi}{\lambda} x\right) y^2$$

where (u, v) are the velocity components in the streamwise and normal directions, respectively; A is the nondimensional shear rate; and λ is the nondimensional wavelength. Values of these parameters can be obtained from the multiscale analysis presented above. This velocity field was then imposed on the combustion process of a homogeneous propellant where the reactions are modeled using a one-step global kinetic scheme.

Figure 12 shows the reaction rate contours as a function of A. Note that as the parameter increases, the flame structure becomes distorted. The perturbation stretches the flame and at a sufficiently large value of A (but still well within physical reality), the flame becomes locally quenched. As a result, part of the flame moves appreciably closer to the injection surface, increasing the local heat flux to the surface, while part of the flame moves away from the surface, decreasing the local heat flux to the surface. Thus, there is a competition between the local regions where the heat flux is increased with regions where the local heat flux is decreased. This competition leads to the existence of a threshold between negative and positive erosive burning. Figure 13 plots the erosive burning rate

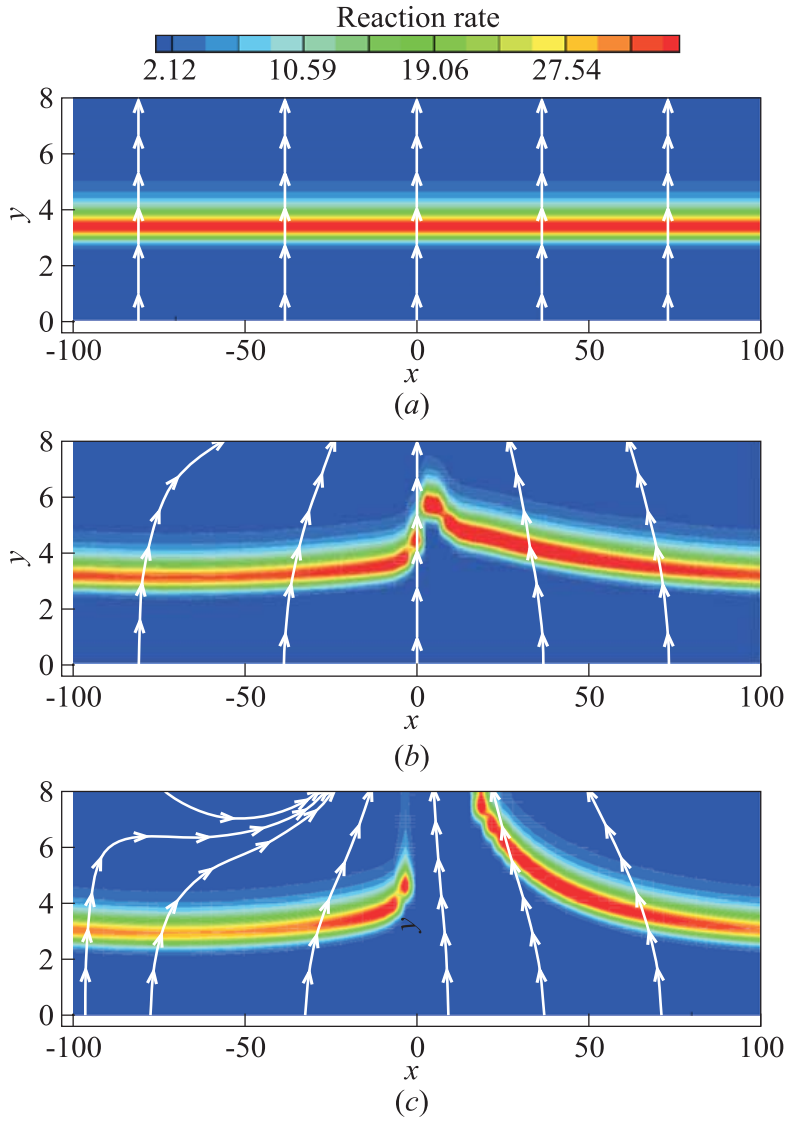

Figure 12 Reaction rate contours with amplitudes of $A = 0$ (*a*); 0.5 (*b*); and 1 (*c*). Streamlines of the imposed velocity field are shown as white curves. (Refer Jackson, p. 16.)

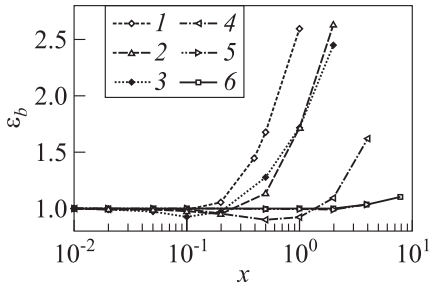

Figure 13 Erosive burning rate coefficient as a function of A for different values of δ and λ: $\lambda = 20$: *1* — $\delta = 5 \cdot 10^5$; $\lambda = 40$: *2* — $\delta = 5 \cdot 10^5$; and $\lambda = 200$: *3* — $\delta = 4 \cdot 10^5$; *4* — $5 \cdot 10^5$; *5* — $2 \cdot 10^6$; and *6* — $\delta = 10^7$

coefficient as a function of the parameter A for different values δ and λ; δ is a measure of the flame standoff distance and is related to the pressure. Note that the erosive burning coefficient can be greater than or less than 1, in agreement with published experimental data [24, 25]. More details can be found in [26].

Heterogeneous propellants

For heterogeneous propellants, the multiscale analysis suggests that the shear near the propellant surface is only time dependent, since the spatial scales are much larger than a typical AP particle diameter. Therefore, the shear was modeled via $u = A \sin(2\pi f t) y$ where A (1/s) is the shear rate; f is the frequency; t is the time; and y is the coordinate in the normal direction to the nominal propellant surface (see [27, 28] for more details).

Figure 14*b* shows a 2D polydisperse pack of 200-micron diameter AP, and Fig. 14*a* shows the surface-averaged burn rate as a function of propellant burnt over two periods for two different shear amplitudes and for $f = 100$ Hz at 30 atm. The average burn rates are 0.3606 and 0.704 cm/s, respectively. The burn rate coefficient, $\varepsilon_b = r_b / r_{bo}$ where r_{bo} is the nominal burn rate, is plotted in Fig. 14*b*, and shows significant erosive burning. Comparisons to experimental data will need to wait until 3D simulations are carried out.

ACKNOWLEDGMENTS

This work has been supported from a variety of sources over the past decade, but the main sources of support are from the U.S. Department of Energy through the University of California under subcontract B523819; a number of grants from

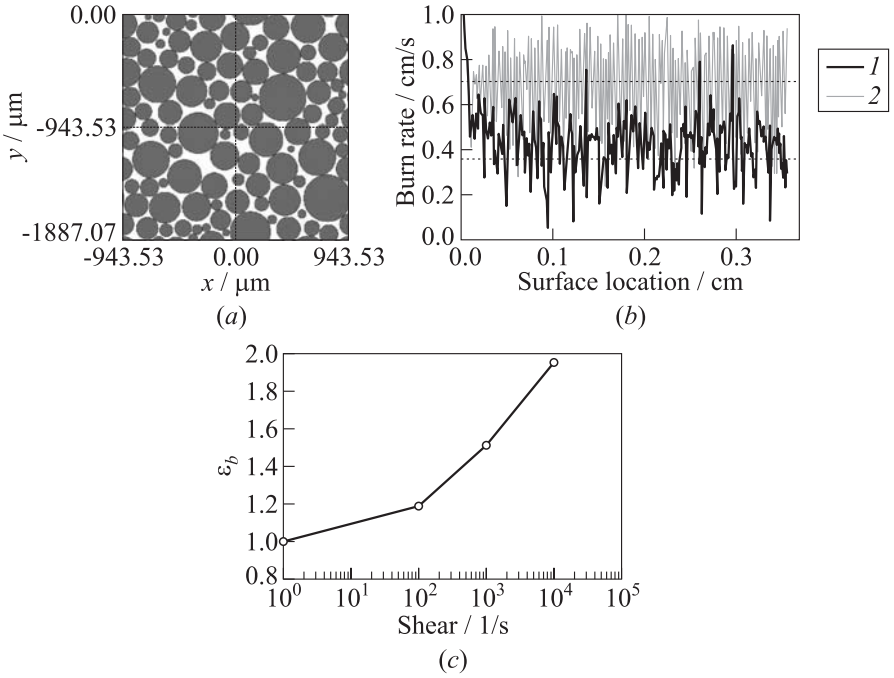

Figure 14 Polydisperse 200-micron pack of disks with volume fraction 0.78 (*a*); surface averaged burn rate as a function of propellant burnt for shear rate amplitudes of 0 (grey) and 10^4 1/s (black) (*b*); and erosive burn rate coefficient as a function of shear amplitude (*c*)

AFOSR, program manager Dr. Arje Nachman; and by the NASA Constellation University Institutes Project under grant NCC3-989 through the University of Maryland with a subcontract Z634015 to University of Illinois at Urbana-Champaign, with Claudia Meyer as the project manager. The author would like also to acknowledge J. Buckmaster, A. Isfahani, V. Topalian, and J. Zhang, whose valuable input and help made this project possible.

REFERENCES

1. Lubachevsky, B. D., and F. H. Stillinger. 1990. Geometric properties of random disk packings. *J. Stat. Phys.* 60(5):561–83.
2. Wang, X., J. Buckmaster, and T. L. Jackson. 2006. The burning of ammonium-perchlorate ellipses and spheriods in fuel binder. *J. Propul. Power* 22(4):764–68.

3. Miller, R. R. 1982. Effects of particle size on reduced smoke propellant ballistics. AIAA Paper No. 82-1096.
4. Knott, G. M., T. L. Jackson, and J. Buckmaster. 2001. The random packing of heterogeneous propellants. *AIAA J.* 39(4):678–86.
5. Kochevets, S., J. Buckmaster, T. L. Jackson, and A. Hegab. 2001. Random packs and their use in the modeling of heterogeneous solid propellant combustion. *J. Propul. Power* 17(4):883–91.
6. Maggi, F., S. Stafford, T. L. Jackson, and J. Buckmaster. 2008. Nature of packs used in propellant modeling. *Phys. Rev. E.* 77:046107.
7. Chen, M., J. Buckmaster, T. L. Jackson, and L. Massa. 2002. Homogenization issues and the combustion of heterogeneous solid propellants. *Proc. Combust. Inst.* 29:2923–29.
8. Massa., L., T. L. Jackson, and J. Buckmaster. 2005. New kinetics for a model of heterogeneous propellant combustion. *J. Propul. Power* 21(5):914–24.
9. Massa, L., T. L. Jackson, and J. Buckmaster. 2007. Optimization of global kinetics parameters for heterogeneous propellant combustion using a genetic algorithm. *Combust. Theory Model.* 11(4):553–68.
10. Wang, X., T. L. Jackson, and L. Massa. 2004. Numerical simulation of heterogeneous propellant combustion by a level set method. *Combust. Theory Model.* 8:227–54.
11. Wang, X., and T. L. Jackson. 2005. The numerical simulation of two-dimensional aluminized composite solid propellant combustion. *Combust. Theory Model.* 9:171–97.
12. Wang, X., K. Hossain, and T. L. Jackson. 2008. The three-dimensional numerical simulation of aluminized composite solid propellant combustion. *Combust. Theory Model.* 12(1):45–71.
13. Massa, L., T. L. Jackson, J. Buckmaster, and F. Najjar. 2007. Fluctuations above a burning heterogeneous propellant. *J. Fluid Mech.* 581:1–32.
14. Massa, L., and T. L. Jackson. 2008. Multidimensional numerical simulation of AP-based propellant combustion with fine/ultrafine aluminum. *J. Propul. Power* 24(2):161–74.
15. Wang, X., T. L. Jackson, and J. Buckmaster. 2007. Numerical simulation of the three-dimensional combustion of aluminized heterogeneous propellants. *Proc. Combust. Inst.* 31:2055–62.
16. Buckmaster, J., T. L. Jackson, L. Massa, and M. Ulrich. 2005. Response of a burning heterogeneous propellant to small pressure disturbances. *Proc. Combust. Inst.* 30:2079–86.
17. Daimon, Y., T. L. Jackson, V. Topalian, J. Freund, and J. Buckmaster. 2009. Effect of propellant morphology on acoustics in a planar rocket motor. *Theor. Comput. Fluid Dyn.* 23:63–77.
18. Massa, L., T. L. Jackson, and J. Buckmaster. 2004. Using heterogeneous propellant burning simulations as subgrid components of rocket simulations. *AIAA J.* 42(9):1889–900.
19. Flandro, G. A. 1995. Effects of vorticity on rocket combustion stability. *J. Propul. Power* 11(4):607–25.

20. Roh, T. S., I. S. Tseng, and V. Yang. 1995. Effects of acoustic oscillations on flame dynamics of homogeneous propellants in rocket motors. *J. Propul. Power* 11(4):640–50. (Value of shear rate provided by V. Yang, private communication.)
21. Zhao, Q., P. L. Staab, D. R. Kassoy, and K. Kirkkopru. 2000. Acoustically generated vorticity in an internal flow. *J. Fluid Mech.* 413:247–85.
22. Spalart, P. 1988. Direct simulation of a turbulent boundary layer up to Re_θ=1410. *J. Fluid Mech.* 187:61–98.
23. Venugopal, P., R. D. Moser, and F. M. Najjar. 2008. Direct numerical simulation of turbulence in injection driven plane channel flows. *Phys. Fluids* 20:105103.
24. Vilyunov, V. N., and A. A. Dvoryashin 1971. An experimental investigation of erosive burning effects. *Fizika Gorenia i Vzryva* 7(1):45–51.
25. Vilyunov, V. N., and A. A. Dvoryashin. 1973. On the influence of the initial temperature of solid fuel on the effect of negative erosivity. *Fizika Gorenia i Vzryva* 9(4):602.
26. Zhang, J., and T. L. Jackson. 2010. A model for erosive burning of homogeneous propellants. *Combust. Flame* 157(2):397–407.
27. Buckmaster, J., and T. L. Jackson. 2000. The effects of time-periodic shear on a diffusion flame anchored to a propellant. *Combust. Flame* 120(1–2):211–21.
28. Isfahani, A. H. G., J. Zhang, and T. L. Jackson. 2009. The effects of turbulence-induced time-periodic shear on a flame anchored to a propellant. *Combust. Flame* 156(5):1084–98.